Broad-band infrared ellipsometry measurements of the c-axis response of underdoped $YBa_2Cu_3O_{7-\delta}$: Spectroscopic distinction between the normal-state pseudogap and the superconducting gap

C. Bernhard [a,*], Li Yu [a], A. Dubroka [a], K.W. Kim [a], M. Rössle [a], D. Munzar [b], J. Chaloupka [b], C.T. Lin [c], Th. Wolf [d]

[a] Physics Department and Fribourg Center for Nanomaterials, University of Fribourg, Chemin du Musée 3, CH-1700 Fribourg, CH, Switzerland
[b] Institute of Condensed Matter Physics, Faculty of Science, Masaryk University, Kotlárská 2, CZ-61137 Brno, CZ, Czech Republic
[c] Max-Planck-Institute for Solid State Research, Heisenbergstrasse 1, D-70569 Stuttgart, D, Germany
[d] Forschungszentrum Karlsruhe, IFP, D-76021 Karlsruhe, D, Germany

ARTICLE INFO

ABSTRACT

We present broad-band infrared ellipsometry measurements of the c-axis dielectric response of underdoped $YBa_2Cu_3O_{7-d}$ single crystals. Our data provide a clear spectroscopic distinction between the normal-state pseudogap and the superconducting gap. In particular, they establish that different energy scales are underlying the respective redistributions of spectral weight. Furthermore, our data are suggestive of a mutual competition between the two gaps and thus of an extrinsic nature of the pseudogap with respect to superconductivity.

© 2008 Elsevier Ltd. All rights reserved.

The anomalous normal-state properties of the cuprate high-temperature superconductors (HTS) remain the subject of intense debate. The most prominent feature is the so-called "pseudogap", which develops already in the normal state well above the superconducting critical temperature, T_{sc} [1,2]. The origin of the pseudogap and, in particular, its relationship with the energy gap in the superconducting state is one of the most controversially discussed issues in this field. The pseudogap prevails in the underdoped regime of the dome-shaped phase diagram of T_{sc} versus hole doping, p, and has been observed by several techniques like specific heat [3], angle-resolved photo-emission (ARPES) [4,5], c-axis tunneling [6], and also by far-infrared (FIR) spectroscopy [7–9]. These techniques have established important aspects, like its strong k-space anisotropy [4,5] or its rapid rise on the underdoped side [4,9]. Nevertheless, the central question of whether the pseudogap is intrinsic or extrinsic with respect to superconductivity remains unresolved [2,3,5,10,11]. Prominent intrinsic theories are the phase fluctuation model where the pseudogap corresponds to a superconducting state lacking macroscopic phase coherence [12], precursor pairing models where the pair formation occurs at much higher temperature than the condensation [13], and the resonating valence bond theory [14]. The extrinsic models include numerous conventional and exotic spin- and/or charge density wave (SDW, CDW) states [15].

We have recently reported the first broad-band ellipsometry measurements of the c-axis conductivity of $RBa_2Cu_3O_{7-\delta}$ (R = Y, Nd, La) single crystals, which provide a spectroscopic distinction between the pseudogap and the superconducting gap and suggest that they are independent and likely competitive phenomena [16]. Here we present additional experimental data on underdoped $YBa_2Cu_3O_{7-\delta}$ single crystals, which further substantiate our arguments.

The $YBa_2Cu_3O_{7-\delta}$ crystals were grown in Y-stabilized zirconium crucibles as described in Ref. [17]. Their oxygen contents, δ, and corresponding hole doping of the CuO_2 planes, p, were adjusted by annealing in flowing O_2 and subsequent rapid quenching in liquid nitrogen. The quoted values of T_c (ΔT_c) corresponding to the midpoint (10–90% width) of the diamagnetic transition were determined by SQUID magnetometry. To determine the p values, we employed the empirical relationship, $p = 0.16 \pm \sqrt{(1 - T_c/T_{c,max})/82.6}$, and $T_{c,max} = 92.5$ K [18].

The ellipsometric measurements were performed with a home-built ellipsometer attached to a Bruker Fast-Fourier spectrometer below $700\,cm^{-1}$ at the infrared beamline of the ANKA synchrotron at FZ Karlsruhe, Germany, and at 400–$4000\,cm^{-1}$ with a similar lab-based setup [19,20]. The presented c-axis polarized spectra are corrected for anisotropy effects (due to the layered structure of the high T_c cuprates) using standard numerical procedures [20,21]. Accordingly, each

* Corresponding author. Tel.: +41 26 300 9070.
E-mail address: christian.bernhard@unifr.ch (C. Bernhard).

spectrum is based on a set of two independent measurements with either the *ab*- or the *c*-axis in the plane of incidence (as defined by the incoming and reflected light). Ellipsometry measures the complex dielectric function, $\tilde{\varepsilon}(\omega) = \varepsilon_1(\omega) + i\varepsilon_2(\omega)$, and the related optical conductivity, $\tilde{\sigma}(\omega) = (i\omega/4\pi)(1 - \tilde{\varepsilon}(\omega))$, without a need for a Kramers–Kronig analysis [19–21]. Furthermore, it is a self-normalizing and thus very accurate and reproducible technique. Thanks to the large probe depth of the IR radiation of the order of micrometers, which ensures the bulk nature of the observed phenomena, and the availability of powerful sum rules, it provides important complementary information with respect to other spectroscopic techniques, like for example angle-resolved photo-emission (ARPES) or tunneling spectroscopy.

It was previously noticed that, due to the specific electronic structure of the cuprate HTS, the *c*-axis optical spectra provide partially *k*-space-resolved information about the dynamical properties of the charge carriers within the CuO_2 planes. For example, in $YBa_2Cu_3O_7$ the transport across the spacing layers is determined by the hopping parameter $t_\perp \propto (\cos k_x - \cos k_y)^2$ [22,23], which is maximal near the X-point of the Brillouin zone where the electronic correlations are strongest (so-called "hot spot" or antinodal region) and vanishes at the diagonal (so-called "cold spot" or nodal region). It has been shown that the properties of the spacing layers that separate the CuO_2 planes, while they influence the absolute value of the infrared conductivity, do not determine the characteristic spectral features of the *c*-axis conductivity [9]. Concerning the normal-state pseudogap and its evolution with temperature and doping, a close correspondence with the energy gap as observed in ARPES in the vicinity of the antinodal region has been established [9].

Fig. 1 shows broad-band spectra up to $4000\,cm^{-1}$ of the *c*-axis IR conductivity, $\sigma_{1c}(\omega)$, of a moderately underdoped $YBa_2Cu_3O_{6.8}$ single crystal with $p \approx 0.12$ and $T_c = 82(2)\,K$. Representative spectra showing the effects of the normal-state pseudogap and the superconducting gap are displayed in Fig. 1(a and b), respectively. The temperature difference spectra with respect to the one at room temperature, $\Delta\sigma_{1c} = \sigma_{1c}(T) - \sigma_{1c}(300\,K)$, are detailed in Fig. 1(c). The temperature dependence of the integrated spectral weight, $SW_\alpha^\beta = \int_\alpha^\beta \sigma_{1c}(\omega)\,d\omega$, for representative limits is given in Fig. 1(d–f). Corresponding data for a similarly underdoped $NdBa_2Cu_3O_{6.9}$ crystal have been shown in Ref. [16].

In agreement with previous reports, our data show that the pseudogap manifests itself as a gap-like suppression of $\sigma_{1c}(\omega)$ below a crossing point at $\omega_{PG} \approx 680\,cm^{-1}$. Its onset temperature of $T^* \approx 180\,K$ is readily deduced from the onset of the suppression of
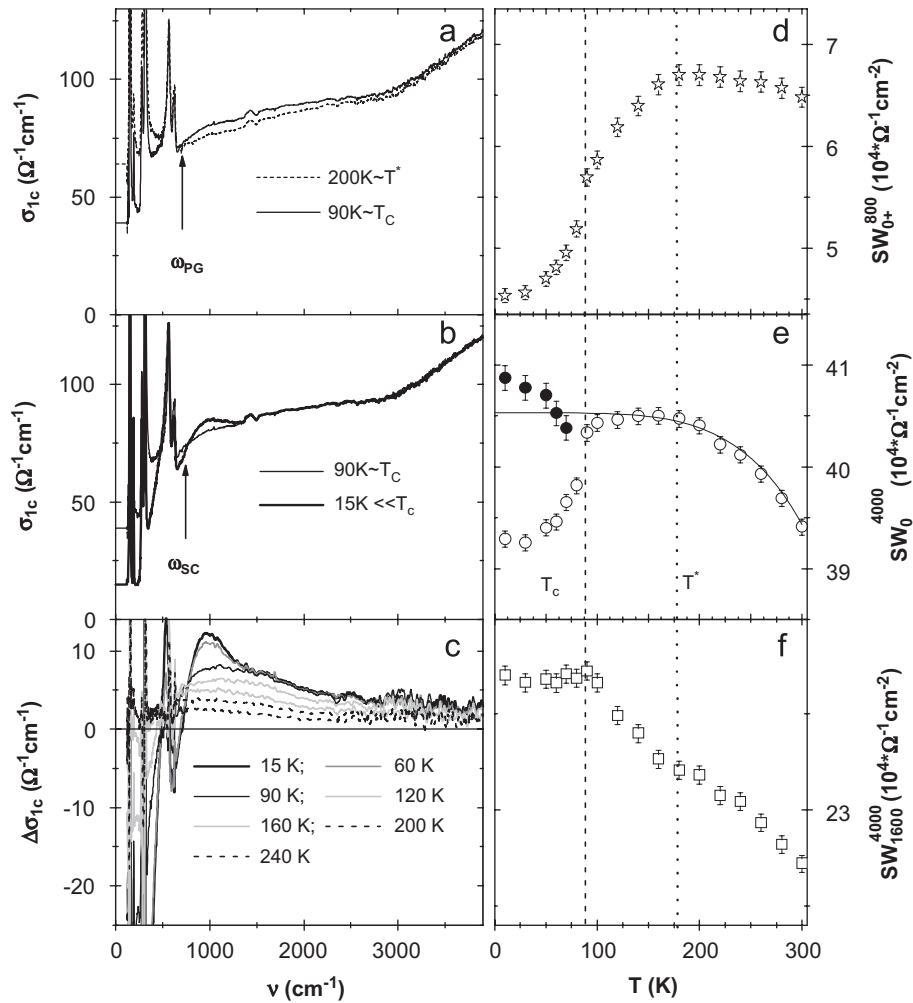
Fig. 1. *c*-axis conductivity of an underdoped $YBa_2Cu_3O_{6.8}$ single crystal with $T_c = 82(2)\,K$ and $p \approx 0.12$. The spectra detail the changes in (a) the pseudogap state, (b) the superconducting state, and (c) the temperature difference, $\Delta\sigma_{1c} = \sigma_{1c}(T) - \sigma_{1c}(300\,K)$. Arrows mark the crossing points at ω_{PG} and ω_{SC}. Also shown is the temperature dependence of the spectral weight, $SW_\alpha^\beta = \int_\alpha^\beta \sigma_{1c}(\omega)\,d\omega$ for (d) $\alpha^+ = 0$ and $\beta = 800\,cm^{-1}$ (regular part), (e) $\alpha = 0$ and $\beta = 4000\,cm^{-1}$ where open circles show the regular part while closed circles include the weight of the SC delta function, SW^δ, and (f) $\alpha = 1600$ and $\beta = 4000\,cm^{-1}$. Vertical bars show the statistical errors. The solid line in (e) shows a fit to the normal-state data with the function $SW(T) = SW(1 - (T/\Theta)^\beta)$.

$SW_{0^+}^{800\,\mathrm{cm}^{-1}}$ with decreasing temperature in Fig. 1(d) (as opposed to the weak increase of $SW_{0^+}^{800\,\mathrm{cm}^{-1}}$ at $T>T^*$). Our broad-band data furthermore establish that the spectral weight that is missing below ω_{PG} is accumulated in the mid-infrared (MIR) range in a fairly broad band that extends from the gap edge at ω_{PG} to about $3500\,\mathrm{cm}^{-1}$. Our ellipsometric data allow us to firmly exclude the possibility that parts of the missing far-infrared spectral weight in the pseudogap state is transferred to lower frequencies. A corresponding narrow Drude peak or delta function might not be captured in our σ_{1c} spectra but it would still show up clearly in ε_{1c} (which is independently measured with ellipsometry) as a downturn to negative values as a function of decreasing frequency (spectra are not shown here). Instead, it is evident from the smooth evolution of $SW_{0^+}^{4000\,\mathrm{cm}^{-1}}$ in the normal state, which unlike $SW_{0^+}^{800\,\mathrm{cm}^{-1}}$ does not exhibit a pronounced decrease below T^*, that the missing far-infrared spectral weight below ω_{PG} is redistributed into the broad MIR band. We note that the increase of $SW_{0^+}^{4000\,\mathrm{cm}^{-1}}$ with decreasing temperature, which is most prominent between 300 and 200 K, is not related to the pseudogap phenomenon. Fig. 1(c) shows that the corresponding changes are only weakly frequency dependent in the infrared spectral range (as opposed to the ones due to the pseudogap formation). Furthermore, we find that it occurs equally well in the c-axis response of optimally doped and even of strongly overdoped samples where the pseudogap phenomenon is entirely absent (spectra are not shown here). The corresponding spectral weight increase in the infrared region is also observed for the in-plane response [25]. Similar temperature dependent changes occur even for metals with weakly correlated charge carrier (albeit their magnitude should be by about one order of magnitude smaller), where they are naturally accounted for by the thermal broadening of the Fermi function. We also note that the remaining minor decrease of $SW_{0^+}^{4000\,\mathrm{cm}^{-1}}$ that set in below 120 K is likely related to a precursor superconducting state. This conjecture is supported by recent Nernst-effect measurements on similarly underdoped Bi-2212 crystals, which reveal an onset of superconducting fluctuation below about 120–130 K [24]. We emphasize that the corresponding spectral weight change is smaller by at least one order of magnitude than the one related to the pseudogap formation. Returning to the pseudogap phenomenon, our data reveal that the corresponding redistribution of spectral weight involves a rather conventional energy scale. For our moderately underdoped sample it is less than $4000\,\mathrm{cm}^{-1}$ or 0.5 eV. The characteristic spectral shape may even lead one to interpret the pseudogap in terms of a charge- or spin density wave [26]. However, such a conventional interpretation is questionable since the pseudogap magnitude does not seem to exhibit a BCS-like temperature dependence, i.e. the pseudogap does not close at T^* but merely fills in with thermally excited states.

Our data furthermore detail how the pseudogap-related spectral weight transfer is affected by the onset of superconductivity, in other words, how the weight of the broad MIR band evolves at $T<T_{\mathrm{sc}}$. This is best seen by focusing on the data at $\omega>1600\,\mathrm{cm}^{-1}$, which are not affected by the appearance of additional superconductivity-induced features, such as the well-known transverse-Josephson-plasma mode near $500\,\mathrm{cm}^{-1}$ (which overlaps here with the phonon mode at $565\,\mathrm{cm}^{-1}$) [27] and the narrow band near $1000\,\mathrm{cm}^{-1}$ whose origin is discussed in Ref. [16]. In the first place, Fig. 1(b and c) shows that $\sigma_{1c}(\omega>1600\,\mathrm{cm}^{-1})$ and thus the broad MIR band exhibit hardly any changes below T_{sc}. Nevertheless, the temperature dependence of $SW_{1600\,\mathrm{cm}^{-1}}^{4000\,\mathrm{cm}^{-1}}$ in Fig. 1(f) reveals that the onset of superconductivity has a significant impact. While $SW_{1600\,\mathrm{cm}^{-1}}^{4000\,\mathrm{cm}^{-1}}$ rapidly increases in the normal state, especially at $T<T^*$, its growth is suddenly interrupted and essentially stopped (within our error bars) below T_{sc}. We note that this characteristic behavior does not depend on the particular choice of the integration limits. The only requirement is that the lower integration limit remains above the onset of the superconductivity-induced band near $1000\,\mathrm{cm}^{-1}$. This trend is also accessible in Fig. 1(c), which shows that the $\Delta\sigma_{1c}$ spectra at 10, 60, and 90 K remain on top of each other for $\omega>1500\,\mathrm{cm}^{-1}$ while the 120 K spectrum already exhibits a clear decrease.

Furthermore, Fig. 2 shows corresponding data for a series of underdoped Y-123 crystals with $T_c=75(2)$, 82(2), and 89(1) K, which establish that this behavior is fairly general. Two important aspects should be emphasized here. Firstly, the onset of superconductivity stops the growth of the broad MIR band and thus the spectral weight transfer associated with the pseudogap formation. On the other hand, the onset of macroscopic superconductivity does not give rise to an inversion of the pseudogap-induced redistribution of spectral weight. Accordingly, our data do not seem to agree with models which assume that the pseudogap corresponds to a precursor superconducting state. The pseudogap effect is caused here by the phase fluctuations of the superconducting order parameter, which should be diminished (or at least noticeably reduced) when the macroscopically coherent state develops below T_{sc}. In contrast to our observation, this should give rise to a (at least partial) superconductivity-induced transfer of spectral weight from the broad MIR band towards low frequency, i.e. to the delta function at the origin, which accounts for the superconducting condensate and the so-called transverse-Josephson-plasma mode [27]. We emphasize that we do not argue here against the existence of precursor superconducting fluctuations, which are meanwhile well established [24]. However, these do not cause the pseudogap phenomenon, rather they seem to be the result of the pseudogap-induced depletion of the low-energy states.

We believe that the superconductivity-induced arrest of the spectral weight of the MIR band is a signature of the competition between the pseudogap and superconductivity for the available low-energy electronic states. In fact, this observation compares rather well with the result of a recent ARPES study [5], which reveals that the pseudogap appears first in the antinodal region from where it expands with decreasing temperature along the Fermi surface. Notably, the expansion of the pseudogap appears to be intersected by the superconducting gap that develops below T_c on the remaining parts (arcs centered around the nodal regions) of the Fermi surface [5]. Accordingly, the combined ARPES and infrared data suggest that the pseudogap and the superconducting gap are competitive and prevail in different parts of the Fermi surface.

Furthermore, our data in Fig. 1 detail the spectral weight redistribution in the superconducting state and thereby confirm a previous report that it involves an unusually high-energy scale [28]. Previously it remained unclear as to whether this high-energy spectral weight redistribution corresponds to a reversal of the pseudogap-related spectral weight transfer. Our data clearly establish that this is not the case since the pseudogap-related spectral weight transfer is limited to the range below $4000\,\mathrm{cm}^{-1}$ while the superconductivity-induced one involves the range above $4000\,\mathrm{cm}^{-1}$. This is evident from Fig. 1(e) where $SW_0^{4000\,\mathrm{cm}^{-1}}$ (solid circles), including the spectral weight of the superconducting delta function, SW^δ, can be seen to exhibit an anomalous increase below T_{sc}. The comparison with the normal-state trend as estimated by a power law fit (solid line) highlights that about 10–20% of SW^δ originate from the frequency range above $4000\,\mathrm{cm}^{-1}$.

Fig. 3 details how the contribution of SW^δ has been deduced. It is important to note that ellipsometry measures independently and directly the real and imaginary parts of the dielectric function, $\varepsilon_1(\omega)$ and $\varepsilon_2(\omega)$, without a need for Kramers–Kronig transformation analysis. SW^δ thus can be readily obtained by fitting with a
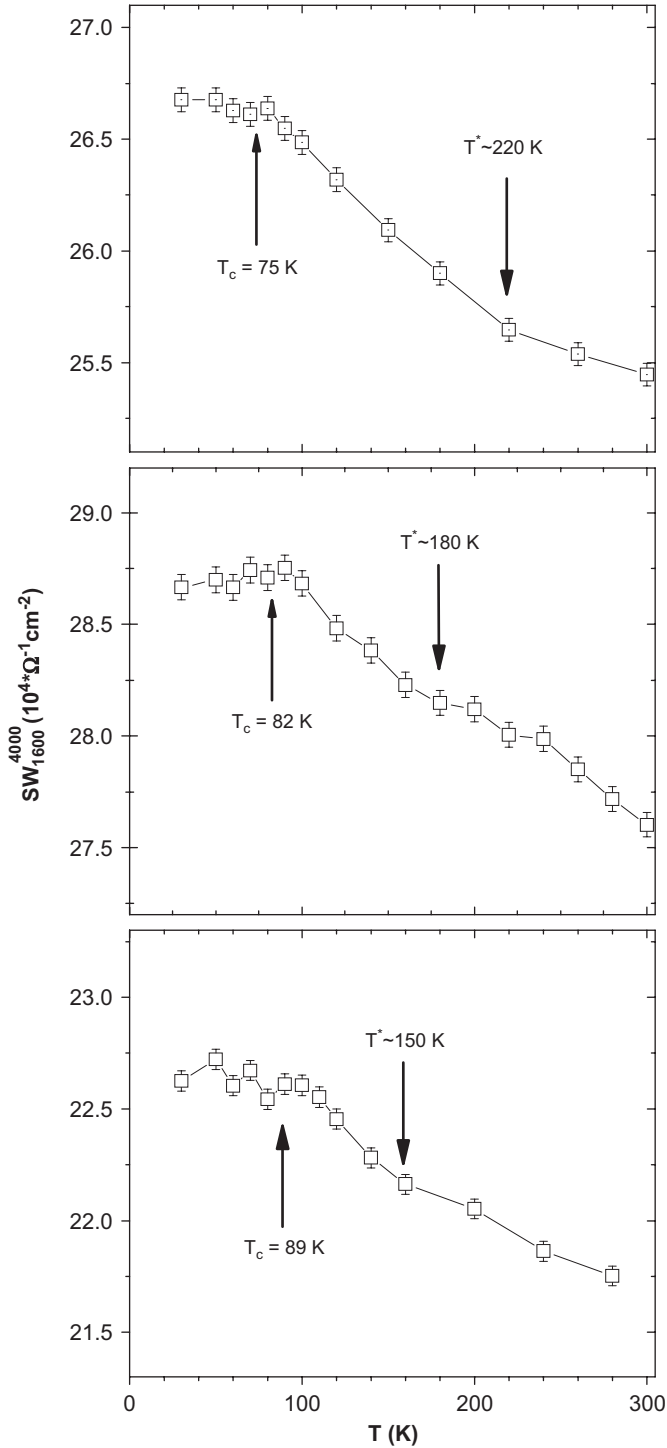
Fig. 2. Temperature dependence of the integrated spectral weight, $SW_{1600}^{4000} = \int_{1600\,\text{cm}^{-1}}^{4000\,\text{cm}^{-1}} \sigma_{1c}(\omega)\,d\omega$, for three differently underdoped YBa$_2$Cu$_3$O$_{7-\delta}$ crystals with $T_c = 75(2)$ K, $82(2)$ K (see also Fig. 1f), and $89(1)$ K. For all three samples the temperature dependence of SW_{1600}^{4000} exhibits a clear anomaly around T_{sc} below which it saturates.

Fig. 3. Determination of the spectral weight of the delta function at the origin, SW^δ, due to the superconducting condensate. Shown is a fit with a Drude–Lorentz model (solid line) to the ellipsometrically measured spectra of the c-axis dielectric function at 10 K (open circles) of the YBa$_2$Cu$_3$O$_{6.8}$ crystal. The dotted line shows ε_{1c} after the subtraction of the contributions of the regular oscillators. Its zero-crossing, as marked by the solid arrow, yields the so-called screened plasma frequency $\tilde{\omega}_{\text{pl,SC}} = \omega_{\text{pl,SC}}/\sqrt{\varepsilon_\infty}$.

In the first term, ε_∞ represents the frequency-independent contribution due to all oscillators that are located well above the upper limit of the fitted frequency range. The value of ε_∞ thus depends on the upper limit of the fitting range. Here the upper limit of 650 cm^{-1} yields $\varepsilon_\infty = 7.8$. For comparison, a value of $\varepsilon_\infty = 4.6$ is obtained with an upper limit of 4000 cm^{-1}. The difference corresponds to the spectral weight of the electronic continuum including the spectral weight of the broad MIR band. The second term represents a sum of Lorentzian oscillators with eigenfrequencies, ω_{0j}, spectral weights, S_j, and half-widths

so-called Drude–Lorentz function:

$$\tilde{\varepsilon}(\omega) = \varepsilon_\infty + \sum_j \frac{S_j \omega_{0j}^2}{\omega_{0j}^2 - \omega^2 - i\omega\gamma_j} - \frac{\omega_{\text{pl,SC}}^2}{\omega(\omega + i\delta(\omega))}$$

$$\text{with} \quad SW^\delta[\Omega^{-1}\,\text{cm}^{-2}] = \frac{\pi}{120}\,\omega_{\text{pl,SC}}^2[\text{cm}^{-2}].$$
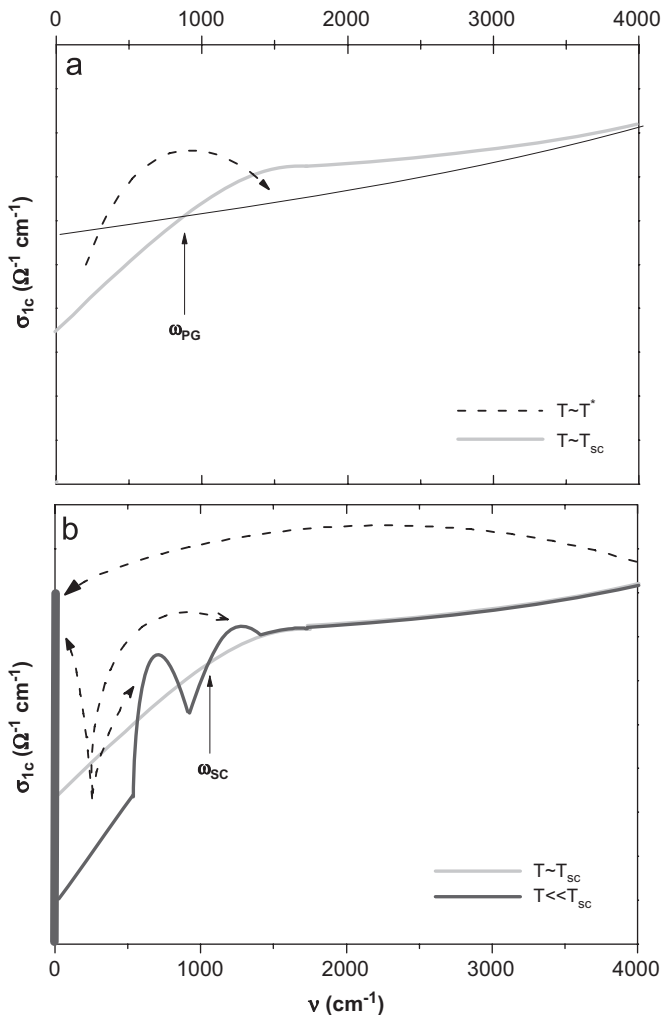
Fig. 4. Sketch summarizing the spectral weight redistributions due to (a) the pseudogap in the normal state at $T_{sc} < T < T^*$ and (b) the gap formation in the superconducting state at $T < T_{sc}$. The dashed arrows indicate the direction of the spectral weight transfer. In (b) the solid thick bar shows the delta function at the origin due to the superconducting condensate. The superconductivity-induced modes at finite frequency are the so-called transverse-Josephson-plasma mode [27] and a mode above the gap edge whose origin is discussed in Ref. [16].

at half-maximum, γ_j. These account for the contributions of the infrared-active phonon modes near 155, 190, 280, 310, 565, and 625 cm^{-1}, the broader superconductivity-induced transverse-Josephson-plasma resonance (t-JPR) mode near 500 cm^{-1} [27] (which strongly overlaps with the phonon mode at 565 cm^{-1}), and the very broad overall electronic background. The third term represents the contribution of the superconducting condensate, which leads to the δ function at the origin in $\sigma_{1c}(\omega)$.

The fit yields $\omega_{pl,SC} = 780(10)$ cm^{-1} and $SW^{\delta} \approx 15,920(400)\,\Omega^{-1}$ cm^{-2}. The latter value corresponds to the difference between the solid and the open circles in Fig. 1(d). The value of $\omega_{pl,SC}$ can also be estimated from the dashed line in Fig. 3(b), which shows the experimental data of ε_{1c} after the contributions of the regular oscillators have been subtracted. The zero crossing near 280 cm^{-1} (as marked by the arrow) corresponds to the so-called screened plasma frequency, $\tilde{\omega}_{pl,SC} = \omega_{pl,SC}/\sqrt{\varepsilon_{\infty}}$. Finally, we note that our value of $\omega_{pl,SC}$ compares reasonably well with the ones obtained from conventional reflection measurements for similarly underdoped YBa$_2$Cu$_3$O$_{7-\delta}$ [29].

Finally, Fig. 4 shows a sketch that summarizes the redistribution of spectral weight due to the formation of the pseudogap in the normal state and the superconducting gap below T_{sc}. We have omitted here the overall spectral weight gain with decreasing temperature which does not exhibit any specific spectral features below 4000 cm^{-1} and which occurs equally well for overdoped samples. We note that the crossing points of the conductivity spectra, marked as ω_{PG} for the pseudogap state and ω_{SC} for the superconducting state, are generally different and doping dependent. This is detailed in Ref. [16], which shows that while ω_{SC} remains nearly constant in a wide range of the underdoped to the optimally doped regime, ω_{PG} decreases rather rapidly as a function of doping. It even crosses ω_{SC} near $p \approx 0.12$ (the doping state of the $T_c = 82$ K sample in Fig. 1) and seems to vanish around the critical point of $p \approx 0.19$.

In conclusion, we have presented broad-band infrared ellipsometry measurements of the c-axis conductivity of underdoped YBa$_2$Cu$_3$O$_{7-\delta}$ single crystals, which provide a clear spectroscopic distinction between the normal-state pseudogap and the superconducting gap. Our data establish that the respective spectral weight redistributions involve different energy scales. In particular, they reveal a pseudogap-induced transfer of spectral weight from low energies to a rather broad mid-infrared band, which is suddenly interrupted by the onset of superconductivity. Accordingly, our data support a two-gap scenario with an extrinsic pseudogap that depletes the low-energy density of states available for superconductivity.

References

[1] T. Timusk, B. Statt, Rep. Prog. Phys. 62 (1999) 61.
[2] (a) J.L. Tallon, et al., Phys. Stat. Sol. (b) 215 (1999) 531;
    (b) J.L. Tallon, J.W. Loram, Physica C 349 (2001) 53.
[3] J.W. Loram, K.A. Mirza, J.R. Cooper, W.Y. Liang, Phys. Rev. Lett. 71 (1993) 1740.
[4] A.G. Loeser, et al., Science 273 (1996) 325.
[5] K. Tanaka, et al., Science 314 (2006) 1910.
[6] V.M. Krasnov, A. Yurgens, D. Winkler, P. Delsing, T. Claeson, Phys. Rev. Lett. 84 (2000) 5860.
[7] C.C. Homes, T. Timusk, R. Liang, D.A. Bonn, W.N. Hardy, Phys. Rev. Lett. 71 (1993) 1645.
[8] D.N. Basov, T. Timusk, Rev. Mod. Phys. 77 (2005) 721.
[9] C. Bernhard, et al., Phys. Rev. B 59 (1999) R6631;
    C. Bernhard, et al., Phys. Rev. Lett. 80 (1998) 1762;
    C. Bernhard, et al., Physica C 317–318 (1999) 276;
    C. Bernhard, et al., Phys. Rev. B 61 (2000) 618;
    C. Bernhard, et al., Phys. Rev. B 62 (2000) 9138;
    A.V. Pimenov, et al., Phys. Rev. Lett. 94 (2005) 227003.
[10] M. Kugler, O. Fischer, C. Renner, S. Ono, Y. Ando, Phys. Rev. Lett. 86 (2001) 4911.
[11] N. Miyakawa, Physica C 364 (2001) 475.
[12] V.J. Emery, S.A. Kivelson, Nature 374 (1995) 434.
[13] I. Kosztin, Q. Chen, Y.J. Kao, K. Levin, Phys. Rev. B 61 (2000) 11662.
[14] P.W. Anderson, et al., J. Phys.: Condens. Matter 16 (2004) R755.
[15] A.V. Chubukov, J. Schmalian, Phys. Rev. B 57 (1998) R11085;
    C.M. Varma, Phys. Rev. Lett. 83 (1999) 3538.
[16] Li Yu, et al., Phys. Rev. Lett. 100 (2008) 177004.
[17] C.T. Lin, W. Zhou, W.Y. Liang, E. Schönherr, H. Bender, Physica C 195 (1992) 291;
    S.I. Schlachter, et al., Int. J. Modern Phys. B 14 (2000) 3673.
[18] J.L. Tallon, et al., Phys. Rev. B 51 (1995) 12911.
[19] A. Golnik, C. Bernhard, J. Humlicek, M. Kläser, M. Cardona, Phys. Stat. Sol. (b) 215 (1999) 553.
[20] C. Bernhard, J. Humlicek, B. Keimer, Thin Solid Films 455–456 (2004) 143.
[21] R.M.A. Azzam, N.H. Bashara, Ellipsometry and Polarized Light, North-Holland, Amsterdam, 1977.
[22] O.K. Andersen, et al., J. Phys. Chem. Solids 56 (1995) 1573.
[23] T. Xiang, J.M. Wheatley, Phys. Rev. Lett. 77 (1996) 4632.
[24] Y. Wang, et al., Phys. Rev. Lett. 95 (2005) 247002.

[25] A. Boris, et al., Science 304 (2004) 708;
M. Ortolani, P. Calvani, S. Lupi, Phys. Rev. Lett. 94 (2005) 067002.
[26] M. Dressel, G. Grüner, Electrodynamics of Solids, Cambridge University Press, Cambridge, UK, 2002;
M. Dressel, Physica C 317–318 (1999) 89.

[27] D. Munzar, et al., Solid State Commun. 112 (1999) 365;
M. Grüninger, D. van der Marel, A.A. Tsvetkov, A. Erb, Phys. Rev. Lett. 84 (2000) 1575.
[28] D.N. Basov, et al., Science 283 (1999) 49.
[29] C.C. Homes, et al., Phys. Rev. B 71 (2005) 184515.